Thin-Walled Structures 80 (2014) 207–216

Contents lists available at ScienceDirect

Thin-Walled Structures

journal homepage: www.elsevier.com/locate/tws

# Flexural behavior of FRP-HSC-steel composite beams

Yunita Idris, Togay Ozbakkaloglu *

*School of Civil, Environmental and Mining Engineering, University of Adelaide, Australia*

ARTICLE INFO

*Article history:*
Received 9 July 2013
Received in revised form
18 March 2014
Accepted 18 March 2014
Available online 15 April 2014

*Keywords:*
Fiber reinforced polymer (FRP)
High-strength concrete (HSC)
Beams
Confinement
Flexure
Displacement capacity

ABSTRACT

This paper reports on an experimental study on the flexural behavior of fiber reinforced polymer (FRP)-high-strength concrete (HSC)-steel composite beams. Seven double-skin tubular beam (DSTBs) and a concrete-filled FRP tube (CFFT) with an internal steel I-beam were tested as simply supported beams in four-point bending. The main parameters of the experimental study included the cross-sectional shapes of inner steel reinforcement and external FRP tube, concrete strength, presence (or absence) of concrete filling inside the steel tube, and effects of the use of mechanical connectors on the inner steel tube. The results indicate that DSTBs are capable of developing very high inelastic flexural deformations. However, the results also indicate that slip between the concrete and the steel tube of the DSTB can be relatively large, unless the bond between concrete and steel tube is enhanced through the use of mechanical connectors. The results of the beam tests illustrate that the flexural behavior of DSTBs is influenced significantly by the diameter and thickness of the inner steel tube. Concrete-filling the inner steel tube and increasing the concrete strength increase the flexural capacity of DSTBs without affecting their overall ductility. Furthermore, the shape of the inner steel tube influences both the flexural capacity of DSTBs and the occurrence of slippage between the concrete and the inner steel tube. It is shown that the bond slip between the concrete and inner steel tube can be prevented through the use of mechanical connectors. These results are presented together with a discussion on the influence of the main parameters on the flexural behavior of DSTBs.

© 2014 Elsevier Ltd. All rights reserved.

## 1. Introduction

The use of FRP composites in the form of concrete-filled FRP tubes (CFFTs) for the construction of new high-performance structural members has received significant recent attention, with large numbers of studies reporting on the axial compressive [1–14] and seismic behavior [15–20] of CFFT columns. The flexural behavior of CFFTs has also been the focus of a number of studies [21–24], and a few studies have reported on the flexural behavior of CFFT beams reinforced with steel or FRP bars [25,26].

Following research on CFFTs, a new type of composite system was proposed by Teng et al. (27) in the form of a FRP-concrete–steel double-skin tubular (DST) column (DSTC). This composite system consists of an outer FRP tube enclosing a hollow steel tube with concrete sandwiched in between the FRP and steel components. The resulting column combines the advantages of all three materials to achieve a high-performance structural member. A series of experimental studies have been conducted on the axial compressive behavior of DSTCs [28–33]. The results of these tests have demonstrated that the concrete in DSTCs is confined very efficiently, which in turn results in a highly ductile member behavior. A few studies have also reported on the lateral cyclic behavior of DSTCs that were tested under combined axial compression and lateral deformation reversals [34–36]. Reinforcing the findings of the studies on the compressive behavior of CFFTs, these studies revealed that DSTCs exhibit very high inelastic deformation capacities under simulated seismic loading. To date, only a single study has reported on the flexural behavior of DST beams (DSTBs) [37], which was concerned with the behavior NSC DSTBs manufactured with circular glass FRP external tubes. In agreement with the findings of the studies on DSTCs, Yu et al. [37] reported that DSTBs exhibit a very ductile response under flexure. It was also noted, however, that significant slip occurred between the inner steel tube and surrounding concrete of DSTBs.

Along with the studies on DST beams and columns, a number of studies have also been carried out on a different type of FRP-concrete–steel composite system that comprises CFFTs with inner steel I-beams. These early studies on the axial compressive [38–40] and flexural behavior [41] of this composite system demonstrated some of its desirable properties, including a highly ductile behavior.

As, to date, only a single study has dealt with the flexural behavior of DSTBs and no study has reported on the flexural behavior of HSC

* Corresponding author. Tel.: +61 8 8303 6477; fax: +61 8 8303 4359.
*E-mail addresses:* yidris@civeng.adelaide.edu.au (Y. Idris), togay.ozbakkaloglu@adelaide.edu.au (T. Ozbakkaloglu).

http://dx.doi.org/10.1016/j.tws.2014.03.011
0263-8231/© 2014 Elsevier Ltd. All rights reserved.

www.Farsi.ir

DSTBs, additional studies are required to better understand and be able to model the flexural response of these composite beams. To contribute towards this end, this paper presents the first experimental study on the flexural behavior of HSC DSTBs. The study was aimed at investigating the influence of key parameters on the flexural behavior of DSTBs, with particular emphasis placed on the interface-slip behavior between steel tube and surrounding concrete. In addition, to establish relative performances of the two aforementioned composite systems, the behavior of a FRP-HSC-steel beam that was composed of a CFFT and an inner steel I-beam was also experimentally investigated. The main parameters of the study included the cross-sectional shapes of inner steel reinforcement and external FRP tube, concrete strength, presence (or absence) of concrete filling inside the steel tube, and effects of the use of mechanical connectors to enhance the bond between the steel tube and surrounding concrete. Flexural behaviors of the beams were evaluated using the recorded load–mid-span deflection relationships, with additional data provided by the load–slip relationships measured at the ends of the specimens.

## 2. Experimental program

### 2.1. Test specimens

Six DSTBs with circular external FRP tubes and a DSTB with a square FRP tube were manufactured and tested as simply supported beams in a four-point bending setup under monotonic loading. In addition, a single specimen that was composed of a circular CFFT and an inner steel I-beam (i.e. I-CFFT) was also tested under the same loading conditions. Each of the specimens was designed as a flexural beam with a 150-mm cross-section. The corners of the square CFFT were rounded with a 30-mm radius ($R$). The span, measured between the center lines of the supports, was 1.3 m, and the length of the constant moment region between the two point loads was 0.3 m. Seven of the specimens were manufactured using HSC and one with normal strength concrete (NSC). All the specimens were confined with aramid FRP (AFRP) external tubes. Five of the specimens were reinforced with circular inner steel tubes, two with square inner steel tubes, and one with a steel I-beam. Of the five specimens that were reinforced with circular inner steel tubes, three were reinforced with tubes 114.3 mm in diameter and two with 76.1 mm diameter tubes. One of the smaller-diameter specimens was provided with mechanical connectors along the inner steel tube. Table 1 provides a summary of material and geometric properties of the test specimens, and Fig. 1 illustrates their geometry.

The process of DSTB manufacture started with the manufacturing of the outer FRP tube, followed by placing the inner steel tube inside the FRP tube, which functioned as a stay-in-place form during the concrete pour. Concrete mixtures were poured in the space between FRP tube and the inner steel tube, except for DSTB-3 where the concrete was also poured inside the inner steel tube. The process of beam manufacture is illustrated in Fig. 2, with the properties of each material used in the process supplied in the following section.

## 3. Material properties

### 3.1. FRP tubes

Aramid fibers were used to manufacture the outer FRP tube in all the specimens. The tubes were manufactured using a manual wet lay-up process, which involved wrapping epoxy resin impregnated fiber sheets around precision-cut high-density styrofoam molds in the hoop direction. FRP tubes of HSC DSTBs and I-CFFT were made of 2 layers of FRP, whereas the tube of NSC DSTB had a single layer of FRP. FRP sheets were wrapped around the molds one layer at a time, with an overlap length of 100 mm provided for each layer to prevent premature debonding. The overlap region of each subsequent layer was provided on the opposite face at a 180° interval from the previous overlap region. The tubes were manufactured in a manner that the overlap regions formed continuous lines along the length of DSTBs, which were oriented to correspond to the side faces of the beams. The width of each fiber sheet was 300 mm and a small overlap of around 10 mm was provided along the axial direction only to ensure continuity of the tube. The epoxy resin was applied at the fiber sheet coverage rate of 0.6 L/m$^2$, which resulted in a ply thickness of 0.8 mm for the resulting FRP composite. Table 2 provides the properties of aramid sheets and epoxy resin used in the fabrication of the FRP tubes.

### 3.2. Concrete

Two different concrete mixes were used in the manufacture of the specimens, namely the HSC mix and NSC mix. Both mixes consisted of crushed bluestone as the coarse aggregate with a nominal maximum size of 10 mm. Superplasticizer and silica fume, added at 8% of the binder content by weight, were used in the HSC mix. Test day concrete strengths of the specimens were obtained through concrete cylinders tests. As shown in Table 1, test day strengths of the HSC mixes varied slightly between 82 and 92 MPa, and the strength of the NSC mix was established as 42 MPa.

### 3.3. Steel tubes

Five of the DSTBs had circular inner steel tubes with two different external diameters (i.e. 114.3 and 76.1 mm) and thicknesses (i.e. 6.02 and 3.2 mm). One of the DSTBs with 76.1 mm circular inner steel tube (i.e. DSTB-7) was manufactured with

**Table 1**
Properties of test specimens.

| Specimens | $f'_c$ (MPa) | FRP tube | | Inner steel tube | | | | $A_s/A_c$ |
|---|---|---|---|---|---|---|---|---|
| | | Shape | $n$ | Shape | $D$ (mm) | $t_s$ (mm) | Inner void | |
| DSTB-1 | 92 | Circular | 2 | Circular | 114.3 | 6.02 | Empty | 0.28 |
| DSTB-2 | 92 | Circular | 2 | Circular | 76.1 | 3.2 | Empty | 0.06 |
| DSTB-3 | 91 | Circular | 2 | Circular | 114.3 | 6.02 | Filled | 0.13 |
| DSTB-4 | 42 | Circular | 1 | Circular | 114.3 | 6.02 | Empty | 0.28 |
| DSTB-5 | 84 | Circular | 2 | Square | 100 | 6 | Empty | 0.27 |
| DSTB-6 | 84 | Square | 2 | Square | 100 | 6 | Empty | 0.18 |
| DSTB-7 | 91 | Circular | 2 | Circular | 76.1 | 3.2 | Empty | 0.07[a] |
| I-CFFT | 82 | Circular | 2 | Steel I-beam | As in Fig. 1 | | – | 0.10 |

$f'_c$=concrete strength, $n$=number of FRP layers, $D$=diameter of steel tubes, $t_s$=thickness of steel tubes, $A_s/A_c$=reinforcement ratio.

[a] Includes the area of additional mechanical connectors.

www.iran-archive.com

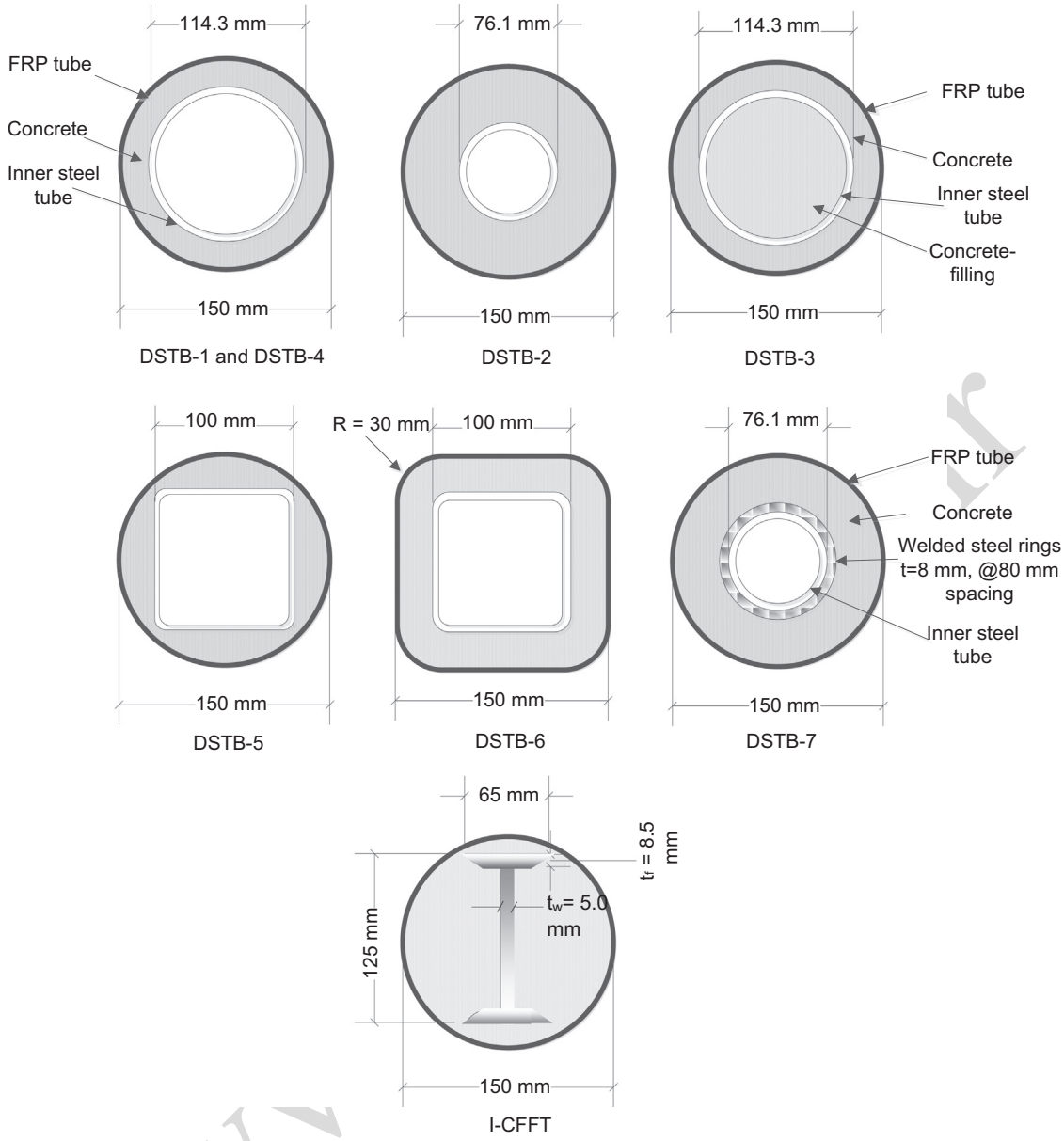


**Fig. 1.** Cross-sections of test specimens.

additional steel rings made of 8-mm diameter steel reinforcement, which were welded on the steel tube along its length at 80-mm spacing. Two of the specimens had a 100 mm square inner steel tube with a thickness of 6 mm. I-CFFT was constructed with an I-beam steel section with a 125 mm height, a flange width of 65 mm, a web thickness of 5 mm, and a tapered flange that varied from 5.5 mm to 8.5 mm in thickness. The exact dimension of the steel I-beam section is shown in Fig. 1. The material properties of the steel tubes were determined by testing five steel coupons cut from the original tube. The coupon specimens of the steel I-beam were cut from the web section as the flanges were tapered. Material properties of inner steel sections, established from coupon tests, are reported in Table 3 together with the properties of 8-mm diameter bars used in DSTB-7, established from direct tension tests.

### 3.4. *Instrumentation, test setup and loading program*

The specimens were instrumented with linear variable displacement transformers (LVDTs) at mid-span, the point of application of concentrated loads, and at the mid-distance between loading points and supports to record the vertical displacements along the beam. Furthermore the specimens were instrumented with 2 additional LVDTs at both ends of specimen to measure the slippage at steel tube–concrete and FRP tube–concrete interfaces. The acquisition of hoop strain data on FRP tubes was of particular interest to better understand the activation of the confinement mechanism and strain distribution at mid-span, two loading points and at mid-distance between loading points and supports. As illustrated in Fig. 3c, 12 strain gauges were bonded to each FRP tube in the hoop direction, and 10 strain gauges were placed axially.

To observe the behavior of the inner steel reinforcement (i.e. steel tubes and I-beam), 10 strain gauges were placed axially at the: (i) mid-span, (ii) two loading points and (iii) one of the sections in the mid-distance between the support and the adjacent loading point (i.e. Section A in Fig. 3c). The 1.3 m long beams were tested using a four-point bending setup. The load was transferred from the actuator to the test beam through a steel loading beam at two locations spaced 0.3 m apart. The load was applied monotonically in displacement control at a rate of

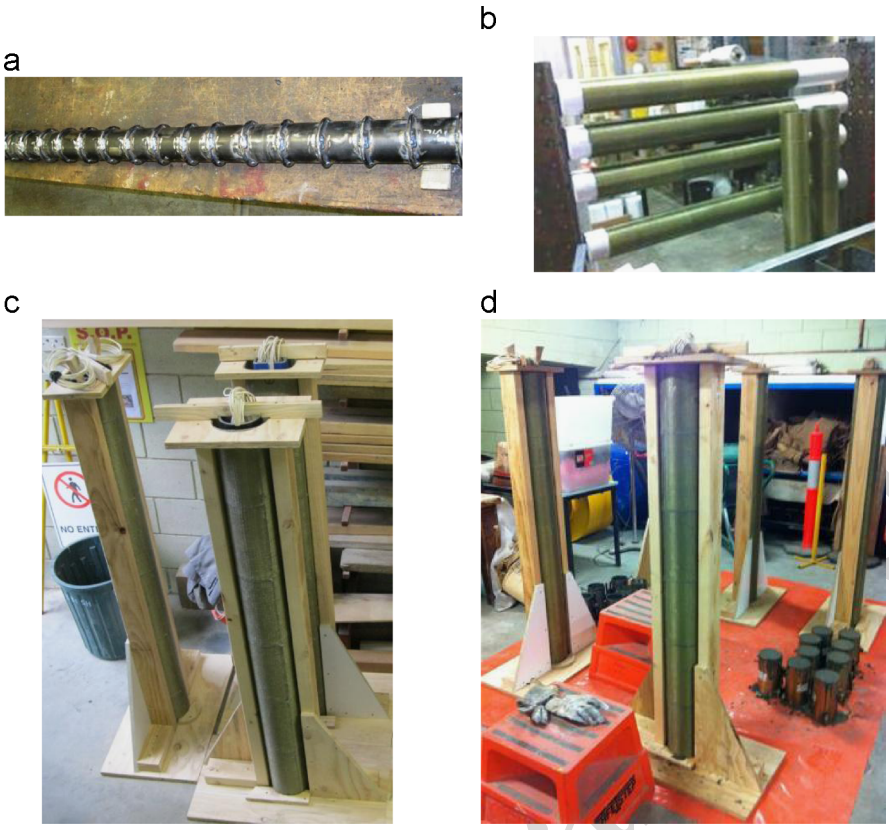


**Fig. 2.** Manufacturing process: (a) steel tubes; (b) manufacturing of FRP tubes; (c) specimens before concrete pouring; (d) specimens after concrete pouring.

**Table 2**
Material properties of fiber sheets and epoxy resin used in FRP tubes.

| Type | Nominal thickness $t_f$ (mm/ply) | Provided by manufacturers | | | Obtained from flat FRP coupon tests | | |
|---|---|---|---|---|---|---|---|
| | | Tensile strength $f_f$ (MPa) | Ultimate tensile strain, $\varepsilon_f$ (%) | Elastic modulus $E_f$ (GPa) | Tensile strength $f_{frp}$ (MPa) | Ultimate tensile strain, $\varepsilon_{frp}$ (%) | Elastic modulus $E_{frp}$ (GPa) |
| Aramid | 0.200 | 2600 | 2.50 | 118.0 | 2390 | 1.86 | 128.5 |
| Epoxy Resin | | > 50 | 2.50 | > 3 | | | |

**Table 3**
Material properties of inner steel sections.

| Steel section | Designation | Yield stress, $f_y$ (MPa) | Ultimate tensile stress, $f_u$ (MPa) | Ultimate tensile strain, $\varepsilon_u$ (%) | Rupture strain, $\varepsilon_r$ (%) |
|---|---|---|---|---|---|
| Tube 1 | 114.3 mm circular | 436 | 490 | 9.5 | 19.4 |
| Tube 2 | 76.1 mm circular | 398 | 483 | 6.9 | 22.0 |
| Tube 3 | 100 mm square | 411 | 470 | 7.7 | 16.5 |
| I-beam | 125 TFB | 418 | 498 | 6.4 | 15.7 |
| Steel rings | 8-mm diameter bars | 546 | 612 | 8.1 | 18.5 |

1 mm/minute. The test setup and instrumentation are illustrated in Fig. 3.

## 4. Test results

### 4.1. Specimens at the end of testing

The tests of all the specimens were stopped after excessive deformation of the specimens, at which point it was no longer possible to maintain symmetrical loading conditions. Fig. 4 illustrates the condition of each specimen after testing, including the most damaged region of the concrete after the removal of FRP tube shell, and the condition of the inner steel reinforcement after the removal of both the FRP tube and concrete.

None of the DSTBs demonstrated any sign of FRP tube rupture. The gap opening along the longitudinal axis of the FRP tubes was observed, which was caused by significant inelastic deformation experienced by the specimens along their mid-span regions. Removal of the FRP tube revealed that the concrete inside the most damaged regions was cracked in several locations along the beam length within the tension region, as shown in Fig. 4. The number and spacing of the concrete

www.Farabi.ir

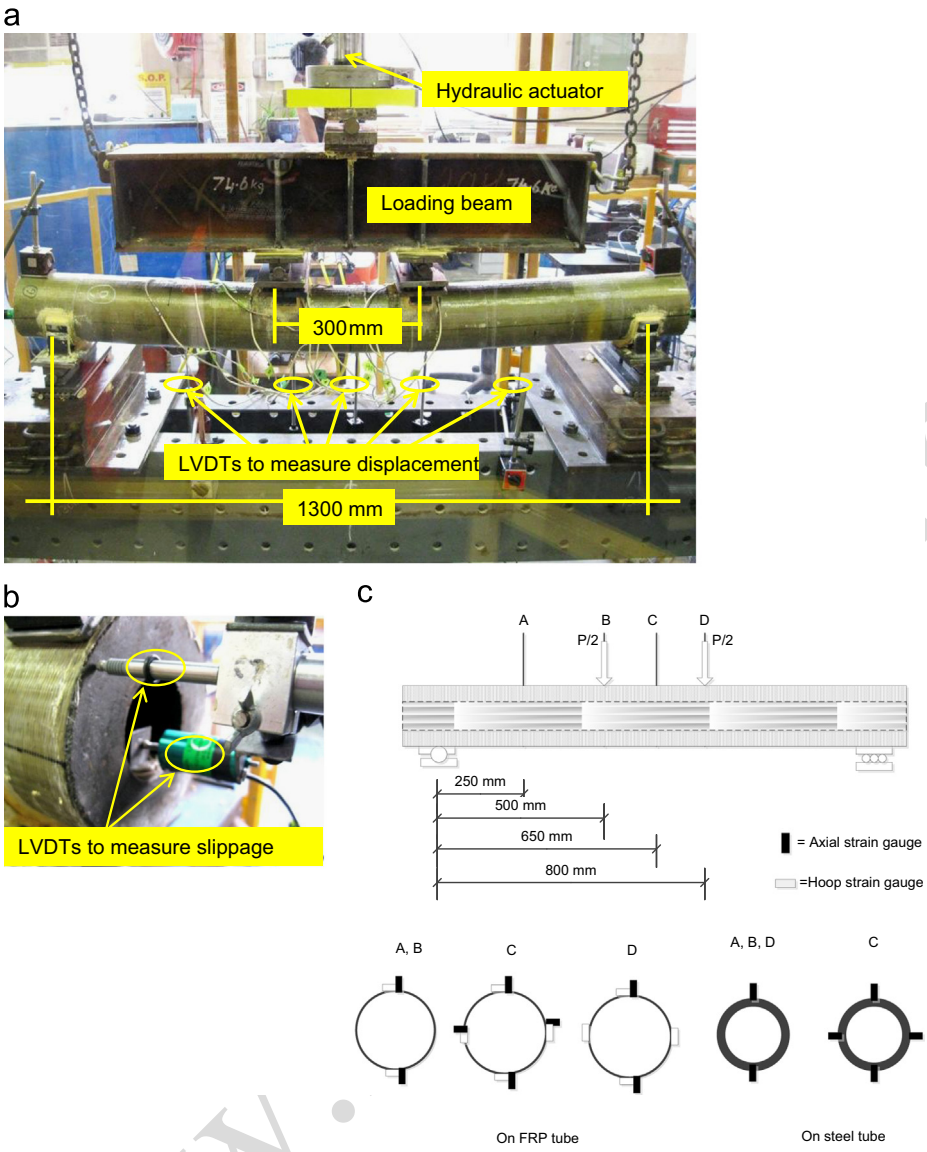


**Fig. 3.** Test setup and instrumentation: (a) illustration of the test setup; (b) locations of LVDTs used to measure slips; (c) strain gauge locations.

cracks were observed to be slightly different for each beam. The presence of mechanical connectors in DSTB-7 resulted in the localization of tension cracking, where the beam developed a single major crack at a location where the inner steel tube exhibited significant plastic deformation. This formation can be attributed to the stronger concrete–steel tube interface bond of DSTB-7, and resulting restraint provided by the inner steel tube against the opening of cracks in concrete. Fig. 4 also shows the condition of the inner steel reinforcements after the removal of the FRP shell and surrounding concrete. As evident from the figure, inner steel reinforcements of all specimens exhibited significant plastic deformation along the constant moment regions of the beams.

### 4.2. Load–deflection relationships

All the specimens showed an almost bi-linear load–deflection relationship with a smooth transition region, as shown in Fig. 5. The majority of the specimens exhibited an almost flat second branch with only a slight decrease in their flexural strengths. The specimen with an inner steel I-beam (I-CFFT), on the other hand, showed a monotonically ascending load–deflection relationship throughout its loading history.

Table 3 provides the recorded data corresponding to the important coordinates of the load–deflection relationships, namely the peak load ($P_{peak}$), recorded mid-span deflection at the peak load ($\Delta_{peak}$), mid-span deflection at ultimate ($\Delta_{ult}$) where testing was stopped, load at ultimate ($P_{ult}$), and steel tube slip. Peak moment ($M_{peak}$) and moment at ultimate ($M_{ult}$), which were calculated from the recorded loads, are also provided in Table 3. A detailed discussion on the influences of the test parameters on the trends of the load–deflection relationships of the DSTBs is provided later in the paper.

### 4.3. Load–slip relationship

#### 4.3.1. Load–slip relationship between concrete and FRP tube

The slips between the FRP tube and concrete was measured by LVDTs that were attached to the FRP tube surface, with the stroke pointed to the concrete section as shown in Fig. 3b. Fig. 6 illustrates the FRP tube–concrete load–slip relationships of the specimens. As evident from Fig. 6, the slip between FRP tube and concrete was insignificant, with a maximum recorded value of 0.06 mm. This finding is in agreement with the one previously reported in Yu et al. [37], and it can be attributed to the fiber


**Fig. 4.** Specimens after testing. (a) DSTB-1, (b) DSTB-2, (c) DSTB-3, (d) DSTB-4, (f) DSTB-5, (g) DSTB-6, (h) DSTB-7 and (i) I-CFFT.

orientation of FRP tubes, which resulted in minimal axial stiffness of the tubes. It might be worth noting that no slippage data was provided for DSTB-3, DSTB-5 and DSTB-6 because of the absence of the instrumentation on these specimens.

### 4.4. Load–slip relationship between concrete and steel tube

The slips between the concrete and the steel tube for each specimen was measured by LVDTs that were attached to the surface of the FRP tubes with the stroke pointed to the inner steel tube, as illustrated in Fig. 3b. These readings were then corrected for FRP tube–concrete slips to obtain the slippage between the steel tube and concrete. The load–slip relationship of each column is provided in Fig. 7. In DSTB-3, with concrete-filled inner steel tube, the load–slip relationship between the steel tube and the inner concrete core was also measured and shown in Fig. 7. In each specimen, the majority of the slippage occurred beyond 75% of maximum recorded load ($P_{peak}$), prior to which slippage was minimal.

The maximum recorded slip among all specimens was around 9 mm, which was observed in DSTB-2, with a 76.1-mm diameter inner steel tube. Increasing the diameter of the inner steel tube to 114.3 mm reduced slippage by around 40%, with DSTB-1 exhibiting 5.5 mm slippage. As illustrated in Fig. 7, there was almost no interface-slip in DSTB-7, which was constructed with a 76.1-mm inner steel tube that was fitted with steel rings. This can be attributed to the increase in the bond strength between the steel tube and concrete due to the mechanical interlock provided by the steel rings, very much like it was observed in the case of deformed bars in concrete (e.g. [42]). Fig. 7 also illustrates that the specimen with an inner steel I-beam (I-CFFT) exhibited almost negligible interface-slip compared to the specimens

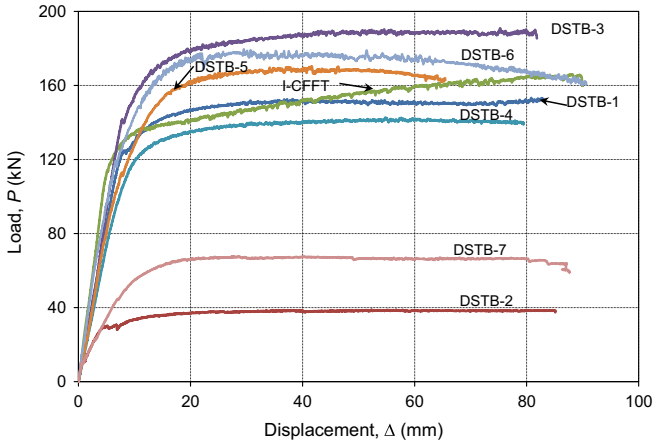


**Fig. 5.** Load–mid-span deflection relationships of DSTBs.

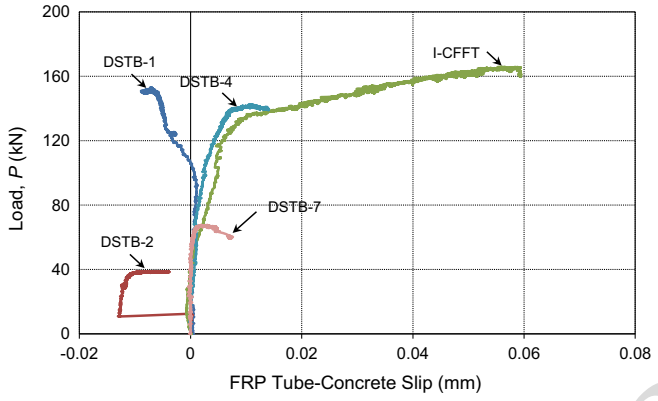


**Fig. 6.** Load–slip relationships measured between FRP tube and concrete.

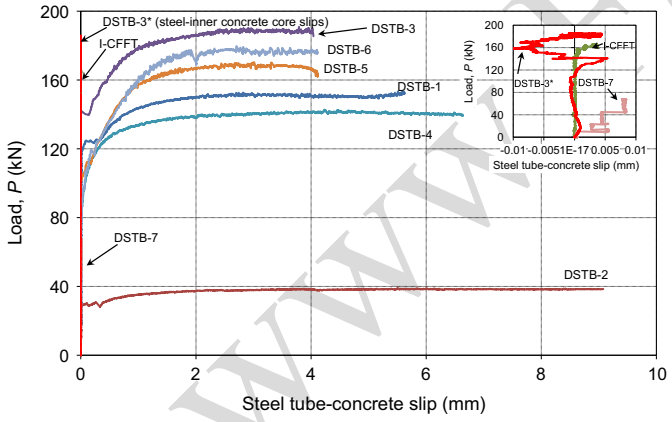


**Fig. 7.** Load–slip relationships between concrete and steel.

having inner steel tubes with no mechanical anchors. This can be explained by the increased relative surface area of the steel I-beam section and the way the steel section was surrounded by the concrete.

As can be seen in Fig. 7, the DSTBs with square inner steel tubes (DSTB-5 and DSTB-6) showed slightly smaller interface-slips than the circular inner steel tube DSTB with a similar cross-sectional area (DSTB-1). Almost identical slips observed in DSTB-5 and DSTB-6 indicates that the cross-sectional shape of the external steel tube had no major influence on the slip behavior of these specimens. It can also be seen in Fig. 7 that the DSTB-4, manufactured with a NSC, exhibited a slightly larger interface-slip than the companion HSC specimen, DSTB-1. Fig. 7 also illustrates that the specimen with a concrete-filled inner steel tube (DSTB-3) exhibited a slightly smaller

**Table 4**
Test results.

| Specimens | $P_{peak}$ (kN) | $M_{peak}$ (kN m) | $\Delta_{peak}$ (mm) | $P_{ult}$ (kN) | $M_{ult}$ (kN m) | $\Delta_{ult}$ (mm) | Steel tube slip (mm) |
|---|---|---|---|---|---|---|---|
| DSTB-1 | 153.2 | 38.3 | 80.8 | 152.4 | 38.1 | 82.6 | 5.6 |
| DSTB-2 | 38.8 | 9.7 | 57.9 | 38.3 | 9.6 | 84.7 | 9.0 |
| DSTB-3 | 190.5 | 47.6 | 75.3 | 188.8 | 47.2 | 81.5 | 4.0 |
| DSTB-4 | 141.9 | 35.4 | 60.6 | 140.2 | 35.1 | 79.5 | 6.6 |
| DSTB-5 | 170.4 | 42.6 | 41.6 | 162.8 | 40.7 | 65.5 | 4.1 |
| DSTB-6 | 179.6 | 44.9 | 29.5 | 161.2 | 40.3 | 90.1 | 4.1 |
| DSTB-7 | 67.7 | 16.9 | 24.3 | 63.7 | 16.0 | 87.1 | 0.008 |
| I-CFFT | 165.6 | 41.4 | 89.5 | 165.6 | 41.4 | 89.5 | 0.004 |

$P_{peak}$=peak load, $\Delta_{peak}$=recorded mid-span deflection at the peak load, $\Delta_{ult}$=mid-span deflection at ultimate, $P_{ult}$=load at ultimate, $M_{peak}$=peak moment, $M_{ult}$=moment at ultimate.

slip that the companion specimen with a hollow inner steel tube (DSTB-1). It can be observed in Fig. 7 that the slip at the interface of the steel tube and inner concrete core that was surrounded by it was negligible. This full bond behavior can be attributed to the high frictional forces developed at this interface, which resulted from the confining forces exerted by the steel tube to the core concrete.

## 5. Analysis and discussion

### 5.1. Influence of test parameters on beam behavior

#### 5.1.1. Effect of diameter and thickness of inner steel tube

The effect of the diameter and thickness of the inner steel tube on the flexural behavior of the DSTBs was investigated by comparing DSTB-1 and DSTB-2. DSTB-1 was reinforced with an inner steel tube 114.3-mm in diameter and 6.02-mm in thickness, whereas DSTB-2 was reinforced with a 76.1-mm diameter inner steel tube with 3.2-mm thickness. DSTB-1 developed a peak load ($P_{peak}$) of 153.2 kN at 80.8 mm mid-span deflection, whereas DSTB-2 was able to sustain a peak load ($P_{peak}$) of only 38.8 kN at 57.9 mm mid-span deflection. These specimens exhibited load–deflection curves with similar trends, both exhibiting almost flat second branches.

#### 5.1.2. Effect of cross- sectional shape of inner steel tube

The effect of cross-sectional shape of inner steel tube was investigated by comparing the behaviors of DSTB-1 (circular inner steel tube) and DSTB-5 (square inner steel tube). The inner steel tubes of these specimens were similar in thickness and cross-sectional area, which resulted in similar reinforcement ratios ($A_s/A_c$) as shown in Table 1. As can be seen in Fig. 5, load–deflection curve of DSTB-5 started exhibiting a slow and steady decline after the attainment of the peak load of 170.4 kN at 41.6 mm mid-span deflection. As illustrated in Table 4, the peak load of DSTB-1 (i.e. 153.2 kN) was lower than that of DSTB-5, but it was attained at a higher mid-span deflection (i.e. 80.8 mm). The higher flexural capacity of DSTB-5 can be attributed to its more efficient inner steel reinforcement placement, with more reinforcement near the extreme tension and compression fibers.

The influence of different forms of inner steel reinforcement was also investigated by comparing I-CFFT with DSTB-3, with a concrete-filled inner circular steel tube. I-CFFT exhibited an ascending second branch in its load–deflection curve, whereas DSTB-3 had a curve with a slightly descending second branch. The peak load of DSTB-3 was 190.5 kN, and it was recorded at 75.3 mm mid-span deflection, whereas I-CFFT reached 165.6 kN of peak load at 89.5 mm mid-span deflection. The higher load capacity of DSTB-3 can be attributed to the higher reinforcement ratio ($A_s/A_c$)

www.IranFire.ir

of the specimen, as shown in Table 1. The hardening type response of I-CFFT compared to the softening response of DSTB-3 suggests that the specimen with an inner steel I-beam had a more favorable neutral axis depth progression compared to the specimen with an inner circular tube resulting in increased moment capacities with increasing deformations.

#### 5.1.3. Effect of FRP tube sectional shape

The effect of the sectional shape of the FRP tube was investigated by comparing DSTB-5 (circular FRP tube) with DSTB-6 (square FRP tube). These specimens were reinforced with identical square inner steel tubes, and they both exhibited load–deflection curve with slightly descending second branches. The peak load of DSTB-5 was 170.4 kN and it was recorded at 41.6 mm mid-span deflection, whereas DSTB-6 reached 179.6 kN of peak load at 29.5 mm mid-span deflection. As expected, due to its larger cross-sectional area the square DSTB exhibited a higher moment capacity. Similar trends of the load–deflection relationships of these specimens suggest that both the circular and the square tube with 30-mm radius of corners provided sufficient confinement leading to a ductile behavior.

#### 5.1.4. Effect of filling the inner steel tube with concrete

The effect of filling the inner steel tube with concrete can be ascertained by comparing the behavior of DSTB-1, which had a hollow inner steel tube with that of DSTB-3, with a concrete-filled inner steel tube. In a similar trend, both specimens showed an almost flat second branch in their load–deflection curves. Due to the increased area of concrete, a higher peak load was recorded for DSTB-3 (190.5 kN at 75.3 mm mid-span deflection) than DSTB-1 (153.2 kN at 80.8 mm of mid-span deflection). These observations indicate that concrete filling of inner steel tube can enhance the flexural capacity of DSTBs, without affecting their ductility.

#### 5.1.5. Effect of concrete strength

The effect of concrete strength on the flexural behavior of the DSTBs was investigated by comparing DSTB-1, which was made of 92 MPa of concrete mix, with DSTB-4 manufactured using 42 MPa concrete. The FRP tubes of these specimens were manufactured using different numbers of FRP layers according to the strength of the concrete to ensure the specimens had similar nominal confinement ratios ($f_{lu}/f'_c$), which were calculated by dividing the ultimate confining pressure ($f_{lu}$) with concrete cylinder strength ($f'_c$):

$$f_{lu} = \frac{2.f_{fu}.t_f}{D} \quad (1)$$

where $f_{f_u}$ = ultimate tensile strength of fibers, $t_f$ = total fiber thickness of the FRP tube, and $D$ = internal diameter of the FRP tube. DSTB-1 was, therefore, confined by two layers of AFRP, whereas DSTB-4 was confined by a single layer of AFRP, which resulted in the nominal confinement ratios ($f_{lu}/f'_c$) of 0.15 and 0.17, respectively.

As mentioned previously, DSTB-1 exhibited a load–deflection relationship with an almost flat second branch, with peak load of 153.2 kN attained at 80.8 mm mid-span deflection. Likewise, the load–deflection relationship of DSTB-4 shown in Fig. 5 illustrates an almost flat post peak behavior, with the peak load of 141.9 kN was attained at 60.6 mm mid-span deflection. The higher maximum load capacity of DSTB-1 over DSTB-4 was expected, and it can be attributed to the higher concrete strength of the former specimen. These results indicate that NSC and HSC DSTBs with similar confinement levels (i.e. $f_{lu}/f'_c$) develop similar inelastic load–deflection behaviors.

#### 5.1.6. Effect of using mechanical connectors

The effect of using mechanical connectors, in the form of steel rings welded on the inner steel tubes, on the flexural behavior of the DSTBs was investigated by comparing DSTB-2 and DSTB-7. Both beams were reinforced with a 76.1-mm diameter inner steel tube, except that the steel inner tube of DSTB-7 was designed with additional steel rings made of 8-mm diameter steel reinforcement with a yield strength of 546 MPa. These rings were welded on the steel tube at 80-mm spacing along its length to increase the bond between the steel tube and concrete. As can be seen in Fig. 5, DSTB-2 and DSTB-7 exhibited an almost identical trend in their load–deflection curves, except DSTB-7 experienced a rapid decline in its capacity around 80 mm mid-span deflection, suggesting that the eventual failure of the specimen was near. Such a declined was not observed in DSTB-2, suggesting that the use of mechanical anchors may result in a reduction in the inelastic deformation capacities of DSTBs. This reduction can be attributed to the elimination of the additional deformations caused by slippage through the use of mechanical connectors.

As evident from Table 4, the addition of mechanical connectors provided a significant increase in specimen flexural capacity, with peak load increasing from 38.8 kN in DSTB-2 to 67.7 kN in DSTB-7. As discussed previously, a significant reduction of slip was recorded for the specimen fitted with the connectors, which changed the partial interaction behavior observed in DSTB-2 to full interaction behavior. The significant portion of the increase in the flexural capacity can be attributed to this change in the bond behavior of the steel tube–concrete interface. In addition, steel rings increased the overall cross-sectional area of the steel reinforcement by approximately 20%, which in turn resulted in a further increase in the flexural capacity of DSTB-7.

### 5.2. Analysis of progression of neutral axis depths

The locations of the neutral axes were established using the maximum strains recorded at the mid-span on the extreme compression and tension fibers of the inner steel tube, established based on the load–axial strain relationships shown in Fig. 8. It is worth noting that the recorded strains were limited to the valid strain gauges readings and it was not possible to obtain complete load–strain curves for all specimens. For this reason the mid-span deflections corresponding to the maximum recorded strains are also provided in Fig. 8. Fig. 9 illustrates variation of the normalized neutral axis depths ($c/D$) with the applied load for all the specimens. The figure illustrates that the neutral axis depths of the specimens initially decreased, and later stabilized at a value below 0.5 in all the specimens.

Fig. 9 illustrates that the $c/D$ values of DSTB-5 with NSC was higher than the companion HSC specimens, DSTB-1. This was

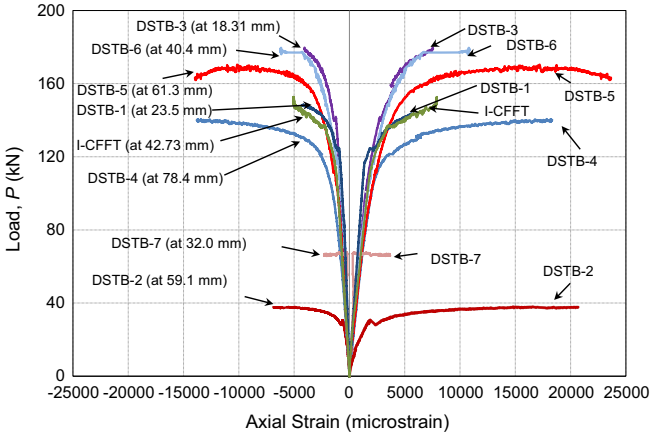


**Fig. 8.** Steel tube axial strains measured at beam mid-span.

www.FarsiBook.ir

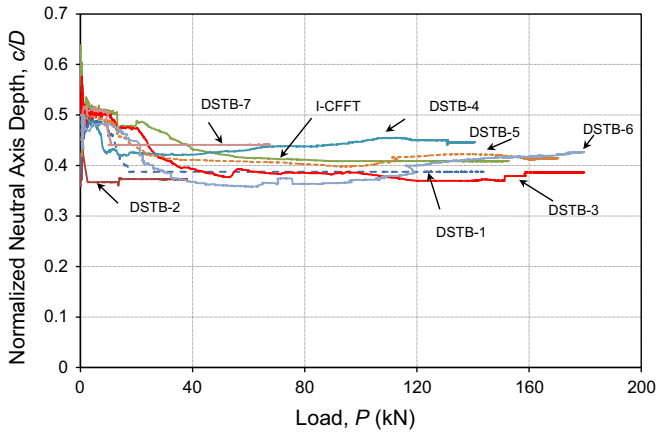


**Fig. 9.** Variation of neutral axis depths.

expected, as in the presence of higher strength concrete sectional force equilibrium is attained at a lower neutral axis depth. The investigation of the neutral axis depths of DSTB-2 and DSTB-7 in Fig. 9 indicates that the neutral axis depth increased with the presence of the mechanical connectors. This can be explained by increased tension forces of the latter specimen resulting from an increased bond at its concrete–steel tube interface due to the presence of mechanical connectors.

The comparison of neutral axis depths of DSTB-5 and DSTB-6 in Fig. 9 shows that DSTB-6 with a square FRP tube had a lower *c/D* ratio until the final stages of testing compared to the companion specimen with a circular FRP tube. This can be attributed to the increased concrete cross-sectional area of the square specimen in the compression zone. The comparison of I-CFFT with DSTB-3, with a concrete-filled inner steel tube, in Fig. 9 indicates that I-CFFT had a higher *c/D* ratio than DSTB-3. This can be explained by the influence of the slightly lower concrete strength of the former specimen and more efficient placement of its inner steel reinforcement, with more reinforcement placed closer to the extreme fibers.

## 6. Conclusions

This paper has presented the results of an experimental study on the flexural behavior of FRP-HSC-steel composite beams. Based on the results presented in the paper, the following conclusions can be drawn:

1. DSTBs exhibit excellent load–deflection behaviors with high inelastic deformations and minimal strength degradations. However, relatively large slips can occur at the concrete–steel tube interface of DSTBs, unless the interface bond is enhanced through the use of mechanical connectors.
2. Like DSTBs, the composite CFFT with an inner steel I-beam investigated in this study is capable of developing a very ductile flexural behavior. Furthermore, unlike DSTBs, this composite system exhibits very little to no slippage at the concrete–steel tube interface.
3. NSC and HSC DSTBs with similar confinement levels ($f_{lu}/f'_c$) develop similar inelastic load–deflection behaviors.
4. FRP tube shape has only a minor influence on the flexural behavior of DSTBs, with companion square and circular specimens demonstrating load–deflection curves with similar general trends.
5. Flexural capacities of DSTBs can be further enhanced through concrete-filling of their inner steel tubes. No detrimental influence of concrete-filling was observed on the ductility of DSTBs.
6. It is observed that increasing the diameter of the inner steel and concrete strength both result in reduced interface-slip between concrete and steel tube, and that DSTBs with square inner steel tubes experience slightly smaller interface-slips compared to the companion circular tubes.
7. Mechanical connectors welded on the inner steel tube along the hoop direction eliminate slippage, which in turn results in a significant increase in the flexural capacity of the DSTB. Therefore, the use of mechanical connectors can be considered as an efficient means for reducing the relatively large slippage that occurs between concrete and inner steel tube of DSTBs.

Because the majority of the specimens of the present study were manufactured with HSC, it is suggested that the above conclusions be considered applicable only to HSC DSTBs until their validity is verified for NSC specimens through additional tests.

## Acknowledgments

The authors would like to thank Messrs. Cai, Wang, Xie and Ms. Tu, who have undertaken the tests reported in this paper as part of their undergraduate theses. This research is part of an ongoing program at the University of Adelaide on FRP-concrete composite members.

## References

[1] Mirmiran A, Shahawy M, Samaan M, El Echary H, Mastrapa JC, Pico O. Effect of column parameters on FRP-confined concrete. J Compos Constr 1998;2(4):175–85.
[2] Fam AZ, Rizkalla SH. Confinement model for axially loaded concrete confined by circular fiber-reinforced polymer tubes. ACI Struct J 2001;98(4):451–61.
[3] Hong WK, Kim HC. Behavior of concrete columns confined by carbon composite tubes. Can J Civ Eng 2004;31(2):178–88.
[4] Fam A, Schnerch D, Rizkalla S. Rectangular filament-wound GFRP tubes filled with concrete under flexural and axial loading: experimental investigation. J Compos Constr 2005;9(1):25–33.
[5] Ozbakkaloglu T, Oehlers DJ. Concrete-filled square and rectangular FRP tubes under axial compression. J Compos Constr 2008;12(4):469–77.
[6] Ozbakkaloglu T, Oehlers DJ. Manufacture and testing of a novel FRP tube confinement. Eng Struct 2008;30(9):2448–59.
[7] Mohamed H, Masmoudi R. Axial load capacity of concrete-filled FRP tube columns: experimental versus predictions. J Compos Constr 2010;14(2):231–43.
[8] Park JH, Jo BW, Yoon SJ, Park SK. Experimental investigation on the structural behavior of concrete filled FRP tubes with/without steel re-bar. KSCE J Civ Eng 2011;15(2):337–45.
[9] Ozbakkaloglu T. Axial compressive behavior of square and rectangular high-strength concrete-filled FRP tubes. J Compos Constr 2013;17(1):151–61.
[10] Ozbakkaloglu T. Compressive behavior of concrete-filled FRP tube columns: assessment of critical column parameters. Eng Struct 2013;51:188–99.
[11] Ozbakkaloglu T. Concrete-filled FRP tubes: manufacture and testing of new forms designed for improved performance. J Compos Constr 2013;17(2):280–91.
[12] Ozbakkaloglu T. Behavior of square and rectangular ultra high-strength concrete-filled FRP tubes under axial compression. Composites B: Engineering 2013;54:97–111.
[13] Vincent T, Ozbakkaloglu T. Influence of concrete strength and confinement method on axial compressive behavior of FRP confined high-and ultra high-strength concrete. Composites B: Engineering 2013;50:413–28.
[14] Vincent T, Ozbakkaloglu T. Influence of fiber orientation and specimen end condition on axial compressive behavior of FRP-confined concrete. Constr Build Mater 2013;47:814–26.
[15] Yamakawa T, Zhong P, Ohama A. Seismic performance of aramid fiber square tubed concrete columns with metallic and/or non metallic reinforcement. J Reinf Plast Compos 2003;22(13):1221–37.
[16] Zhu Z, Ahmad I, Mirmiran A. Seismic performance of concrete-filled FRP tube columns for bridge substructure. J Bridge Eng 2006;11(3):359–70.
[17] Ozbakkaloglu T, Saatcioglu M. Seismic behavior of high strength concrete columns confined by fiber-reinforced polymer tubes. J Compos Constr 2006;10(6):538–49.
[18] Ozbakkaloglu T, Saatcioglu M. Seismic performance of square high strength concrete columns in FRP stay in place formwork. J Struct Eng 2007;133(1):44–56.
[19] Saatcioglu M, Ozbakkaloglu T, Elnabelsy G. Seismic behavior and design of reinforced concrete columns confined with FRP stay-in-place formwork ACI SP257; 2008. p. 145-165.

www.FarFile.ir

[20] Idris Y, Ozbakkaloglu T. Seismic behavior of high-strength concrete-filled FRP tube columns. J Compos Constr 2013;17(6):04013013.
[21] Mirmiran A, Shahawy M, El Khoury C, Naguib W. Large beam-column tests on FRP-filled composite tubes. ACI Struct J 2000;97(2):268–76.
[22] Davol A, Burgueno R, Seible F. Flexural behaviour of circular concrete filled FRP shells. J Struct Eng 2001;127(7):810–7.
[23] Fam AZ, Rizkalla SH. Flexural behavior of concrete filled fiber-reinforced polymer circular tubes. J Compos Constr 2002;6(2):123–32.
[24] Fam AZ, Rizkalla SH. Large scale testing and analysis of hybrid concrete/composite tubes for circular beam-column applications. Constr Build Mater 2003;17(6-7):507–16.
[25] Cole B, Fam A. Flexural load testing of concrete filled FRP tubes with longitudinal steel and FRP rebar. J Compos Constr 2006;10(2):161–71.
[26] Fam A, Cole B, Mandal S. Composite tubes as an alternative to steel spirals for concrete members in bending and shear. Constr Build Mater 2007;21(2):347–55.
[27] Teng JG, Yu T,Wong YL. Behavior of hybrid FRP-concrete-steel double-skin tubular columns. In: Proceedings of the 2nd international conference on FRP composites in civil engineering, Adelaide, Australia; 2004. p. 811–8.
[28] Wong YL, Yu T, Teng JG, Dong SL. Behavior of FRP-confined concrete in annular section columns. CompositesB 2008;39(3):451–66.
[29] Teng JG, Yu T,Wong YL, Hybrid FRP-concrete-steel double-skin tubular structural members. In: Proceedings of the fifth international conference on FRP composites in civil engineering, 27–29 September, Beijing, China; 2010. p. 26–32.
[30] Yu T, Wong YL, Teng JG. Behavior of hybrid FRP-concrete-steel double-skin tubular columns subjected to eccentric compression. Adv Struct Eng 2010;13(5):961–74.
[31] Louk Fanggi BA, Ozbakkaloglu T. Compressive behavior of aramid FRP-HSC-steel double-skin tubular columns. Constr Build Mater 2013;48:554–65.
[32] Ozbakkaloglu T, Louk Fanggi BA. FRP-HSC-steel composite columns: behavior under monotonic and cyclic axial compression. Mater Struct 2013. http://dx.doi.org/10.1617/s11527-013-0216-0.
[33] Ozbakkaloglu T, Louk Fanggi B. Axial compressive behavior of FRP-concrete-steel double-skin tubular columns made of normal- and high-strength concrete. J Compos Constr 2014;18(1):04013027.
[34] Han LH, Tao Z, Liao FY, Xu Y. Tests on cyclic performance of FRP-concrete –steel double-skin tubular columns. Thin-Walled Struct 2010;48(6):430–9.
[35] Zhang B, Teng JG, Yu T. Behaviour of hybrid double-skin tubular columns subjected to combined axial compression and cyclic lateral loading. In: sixth international conference on FRP composites in civil engineering, Rome, Italy; 2012. p 1–7.
[36] Ozbakkaloglu T, Idris Y. Seismic behavior of FRP-high-strength concrete-steel double skin tubular columns. J Struct Eng 2014:04014019, http://dx.doi.org/10.1061/(ASCE)ST.1943-541X.0000981.
[37] Yu T, Wong YL, Dong SL, Lam ESS. Flexural behavior of hybrid FRP-concrete-steel double skin tubular members. J Compos Constr 2006;10(5):443–52.
[38] Karimi K, Tait MJ, El-Dakhakhni WW. Testing and modelling of a novel FRP-encased steel-concrete composite column. Compos Struct 2011;93(5):1463–73.
[39] Karimi K, El-Dakhakhni WW, Tait MJ. Performance enhancement of steel columns using concrete-filled composite jackets. J Perform Constr Facil 2011;25(3):189–201.
[40] Karimi K, Tait MJ, El-Dakhakhni WW. Influence of slenderness on the behaviour of a FRP-encased steel-concrete composite column. J Comp Constr 2012;16(1):100–9.
[41] Zakaib S, Fam A. Flexural performance and moment connection of concrete-filled GFRP tube–encased steel I-sections. J Compos Constr 2012;16(5):604–13.
[42] Park R, Paulay T. Reinforced concrete structures. New York: Wiley; 1975.

www.FaraFile.ir